Wall boundary conditions in the lattice Boltzmann equation method for nonideal gases

Taehun Lee* and Lin Liu
Department of Mechanical Engineering, The City College of the City University of New York, New York, New York 10031, USA
(Received 16 January 2008; published 25 July 2008)

Wall boundary conditions for the lattice Boltzmann equation (LBE) method for nonideal gases proposed by Lee and Fischer [Phys. Rev. E **74**, 046709 (2006)] are examined. The LBE simulations of the contact line are typically contaminated by small but strong counter-rotating parasitic currents near solid surfaces. We find that these currents can be eliminated to round-off if the potential form of the intermolecular force is used with the boundary conditions based on the wall energy approach and the bounce-back rule. Numerical tests confirm the elimination of the parasitic currents in the vicinity of the contact line and the agreement of the calculated density, excess mass, and contact angle at the solid surfaces with theory.

DOI: 10.1103/PhysRevE.78.017702 PACS number(s): 47.11.−j, 47.55.D−, 68.08.Bc

The lattice Boltzmann equation (LBE) simulations of the contact line generate small counter-rotating vortices near solid surfaces [1], which usually become stronger as the contact angle deviates from its neutral value of 90°. The magnitude and spatial extent of the vortices increase with the surface tension force and decrease with the viscous dissipation. Since the vortices do not disappear even in the simulation of the static contact line, they should not be attributed to the mass transfer as an evaporation and condensation process to overcome the singularity of the dynamic contact line or considered as the wedge flow solution [2]. They are the parasitic currents arising from the imbalance between stresses at the liquid-vapor-solid interface, and can be amplified by improper boundary conditions. Since the parasitic currents are numerical artifacts due to discretization errors, they can be avoided if consistent discretization schemes are adopted.

Attempts have been made to reduce the magnitude of the parasitic currents and identify their origins either by revising the formulation of the surface tension force and improving the isotropy of discretization [3–5], or by incorporating the sharp interface dynamics [6,7]. In particular, Lee and Fischer [5] showed that for the van der Waals fluid, use of the potential form of the surface tension force and the isotropic finite difference in the intermolecular force eliminates the parasitic currents to round-off and enables stable simulation of nonideal gas flows with large material property differences.

All of these studies, however, focused on the reduction or elimination of the parasitic currents without considering the effects of wall boundaries. Although the numerical experiments on the contact angles with the LBE methods have been quite successful [1,8–20], the elimination of the parasitic currents and the prediction of the wall density profile have not received much attention. In the external forcing approaches [8–11], mass conservation across the boundary nodes can be easily violated because of the nonzero chemical potential gradient in the direction normal to the boundary. In the coating approaches [12,13], the solid surface is coated with fluid in such a way as to yield the desired contact angle, but the density of the coating fluid may be inconsistent with the wall density determined from minimization of free energy. Density is expected to take higher values than that of the bulk phase at the wetting surface due to attraction and lower values at the nonwetting surface due to repulsion [14]. Failure to satisfy mass conservation or to predict correct wall density distribution would result in strong and localized parasitic currents in the vicinity of the contact line.

In this Brief Report, we propose boundary conditions based on the wall energy approach [17–21] for the accurate prediction of the contact angle and wall density distribution, and the bounce-back rule with equilibrium condition for the mass conservation. We derive the wall boundary condition for the intermolecular forcing term that is consistent with the bounce-back rule. The equilibrium contact angle and density distribution of a static drop on solid surfaces with different wetting characteristics will be examined and compared with theory. It will also be shown that the parasitic currents are eliminated in the presence of wall boundaries.

The discrete Boltzmann equation (DBE) for the van der Waals fluid with Bhatnagar-Gross-Krook (BGK) collision operator [22] was proposed by He *et al.* [23] and can be written as

$$\frac{\partial f_\alpha}{\partial t} + \mathbf{e}_\alpha \cdot \nabla f_\alpha = -\frac{f_\alpha - f_\alpha^{eq}}{\lambda} + \frac{(\mathbf{e}_\alpha - \mathbf{u}) \cdot \mathbf{F}}{\rho c_s^2} f_\alpha^{eq}, \tag{1}$$

where f_α is the particle distribution function, $\mathbf{e}_\alpha$ is the microscopic particle velocity, $\mathbf{u}$ is the macroscopic velocity, ρ is the density, c_s is the speed of sound, λ is the relaxation time, and f_α^{eq} is the equilibrium distribution function [24]. In the above, $\mathbf{F}$ models the intermolecular attraction and the effects of the exclusion volume of the molecules on the equilibrium properties of a dense gas, which can be expressed in the potential form to avoid development of the parasitic currents [5],

$$\mathbf{F} = \nabla \rho c_s^2 - \rho \nabla (\mu_0 - \kappa \nabla^2 \rho), \tag{2}$$

where κ is the gradient parameter, μ_0 is the chemical potential, and κ is the gradient parameter. The equilibrium properties of a system without a wall boundary can be described by a bulk free energy $\Psi_b = \int_\Omega [E_0(\rho) + \kappa |\nabla \rho|^2 / 2] d\Omega$. In the pseudo–van der Waals fluid, E_0 can be approximated by

*thlee@ccny.cuny.edu. URL: http://www-me.ccny.cuny.edu/faculty/lee.html

$E_0(\rho)=\beta(\rho-\rho_v^{sat})^2(\rho-\rho_l^{sat})^2$ [25]. Given the interface thickness D, the constant β, and the saturation densities ρ_v^{sat} and ρ_l^{sat}, the gradient parameter κ and the liquid-vapor surface tension force σ can be computed as $\kappa=\beta D^2(\rho_l^{sat}-\rho_v^{sat})^2/8$ and $\sigma=(\rho_l^{sat}-\rho_v^{sat})^3/6\sqrt{2\kappa\beta}$, respectively. In Eq. (2), the chemical potential is related to E_0 by $\mu_0=\partial_\rho E_0$ and the pressure by $p_0=\rho\partial_\rho E_0-E_0$, which leads to $\nabla p_0=\rho\nabla\mu_0$. In [25], it was shown that the free energy of a closed system filled with the van der Waals fluid decreases due to viscous effects. If the pressure form replaces the potential form, however, inexact satisfaction of $\nabla p_0=\rho\nabla\mu_0$ in the discretized equations prevents a system from reaching equilibrium causing the parasitic currents in the direction normal to the phase interface, while nonisotropic discretizations trigger the parasitic currents with organized eddies. For a detailed discretization of Eqs. (1) and (2) without wall boundaries, see [5].

The boundary condition for the second derivative can be established by considering an additional wall free energy $\Psi_s=\phi_0-\phi_1\rho_s+\cdots$ [21], where ρ_s is the density at the solid surface. Then, the total free energy takes the following form [19]:

$$\Psi_b+\Psi_s=\int_\Omega\left(E_0(\rho)+\frac{\kappa}{2}|\nabla\rho|^2\right)d\Omega-\int_\Gamma(\phi_1\rho_s)d\Gamma, \quad (3)$$

where only the linear term of Ψ_s is taken. At equilibrium, we have two stable solutions that satisfy $-\phi_1=\pm\sqrt{2\kappa E_0(\rho)}$. In terms of the dimensionless wetting potential defined as $\Omega=4\phi_1/(\rho_l^{sat}-\rho_v^{sat})^2\sqrt{2\kappa\beta}$, equilibrium densities at the solid surface in contact with liquid and vapor phases are expressed, respectively, as

$$\rho_{s,l}=\frac{\rho_l^{sat}+\rho_v^{sat}+(\rho_l^{sat}-\rho_v^{sat})\sqrt{1+\Omega}}{2},$$

$$\rho_{s,v}=\frac{\rho_l^{sat}+\rho_v^{sat}-(\rho_l^{sat}-\rho_v^{sat})\sqrt{1-\Omega}}{2}. \quad (4)$$

The dimensionless wetting potential is related to the equilibrium contact angle θ_{eq} by

$$\Omega=2\,\mathrm{sgn}\left(\frac{\pi}{2}-\theta_{eq}\right)\left\{\cos\left(\frac{\alpha}{3}\right)\left[1-\cos\left(\frac{\alpha}{3}\right)\right]\right\}^{1/2}, \quad (5)$$

with $\alpha=\arccos(\sin\theta_{eq})^2$. This imposes the boundary condition for $\nabla^2\rho$ in Eq. (2) as $\kappa\mathbf{n}\cdot\nabla\rho_s=-\phi_1$, where $\mathbf{n}$ is the unit outward normal vector. Once the boundary condition for $\nabla^2\rho$ is prescribed, $\mu=\mu_0-\kappa\nabla^2\rho$ is treated as a scalar.

For the unknown particle distribution function at the solid surface, the equilibrium boundary condition is imposed [26], in which ρ_s is calculated according to the bounce-back rule after streaming, followed by immediate relaxation toward the equilibrium state with the density and velocity at the solid surface. This procedure is further illustrated as follows. Suppose $\mathbf{e}_{\bar{\alpha}}$ is in the direction opposite to $\mathbf{e}_\alpha$ and $f_{\bar{\alpha}}(\mathbf{x}_s)=f_\alpha(\mathbf{x}_s)$ is imposed by the bounce-back rule, where $\mathbf{x}_s$ denotes a grid point populated at the solid surface. Since the streaming step is the exact solution of the pure advection equation $\partial_t f_\alpha+\mathbf{e}_\alpha\cdot\nabla f_\alpha=0$, the bounce-back rule implies $\partial_t f_{\bar{\alpha}}(\mathbf{x}_s)=\partial_t f_\alpha(\mathbf{x}_s)$, which yields $\mathbf{e}_{\bar{\alpha}}\cdot\nabla f_{\bar{\alpha}}(\mathbf{x}_s)=\mathbf{e}_\alpha\cdot\nabla f_\alpha(\mathbf{x}_s)$. After the bounce-back condition is applied, $f_{\bar{\alpha}}(\mathbf{x}_s)$ immediately relaxes toward $f_{\bar{\alpha}}^{eq}(\mathbf{x}_s)$. Thus, an alternative expression of the bounce-back rule can be written for $\mathbf{e}_{\bar{\alpha}}\cdot\nabla f_{\bar{\alpha}}(\mathbf{x}_s)$ as $f_{\bar{\alpha}}^{eq}(\mathbf{x}_s)-f_{\bar{\alpha}}^{eq}(\mathbf{x}_s+\mathbf{e}_\alpha\delta t)=f_\alpha^{eq}(\mathbf{x}_s)-f_\alpha^{eq}(\mathbf{x}_s-\mathbf{e}_\alpha\delta t)$, in which $\mathbf{x}_s+\mathbf{e}_\alpha\delta t$ is located outside the computational domain and is unavailable. As $\mathbf{u}=0$ at $\mathbf{x}_s$, $f_{\bar{\alpha}}^{eq}(\mathbf{x}_s)=f_\alpha^{eq}(\mathbf{x}_s)$ and $f_{\bar{\alpha}}^{eq}(\mathbf{x}_s+\mathbf{e}_\alpha\delta t)=f_\alpha^{eq}(\mathbf{x}_s-\mathbf{e}_\alpha\delta t)$. It can be shown that the first term in Eq. (2) reduces to $(\mathbf{e}_\alpha-\mathbf{u})\cdot\nabla\rho c_s^2 f_\alpha^{eq}(\mathbf{x}_s)/\rho c_s^2=\mathbf{e}_\alpha\cdot\nabla f_\alpha^{eq}(\mathbf{x}_s)$ at $\mathbf{x}_s$. This requires that the directional derivative of the density at the solid surface use the identical discretization to that for the equilibrium distribution function

$$\rho(\mathbf{x}_s)-\rho(\mathbf{x}_s+\mathbf{e}_\alpha\delta t)=\rho(\mathbf{x}_s)-\rho(\mathbf{x}_s-\mathbf{e}_\alpha\delta t). \quad (6)$$

The same condition is imposed for μ. Equation (6) prevents unphysical mass and momentum transfer through the boundary nodes.

The test cases confirm that the LBE method with the consistent boundary conditions is able to reach an equilibrium at different contact angles. All the results presented are obtained for a D2Q9 lattice [24]. Figure 1 shows equilibrium

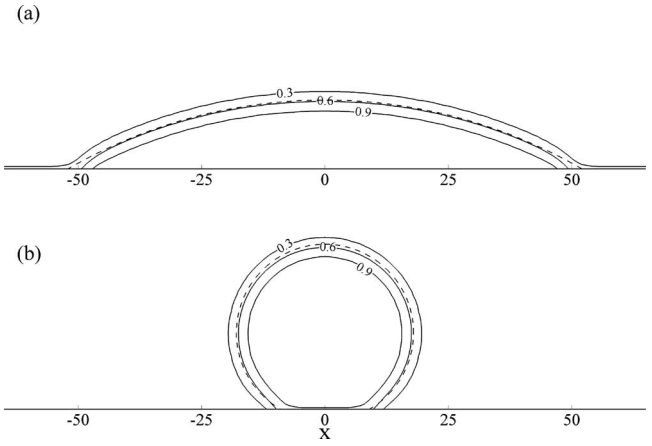

FIG. 1. Equilibrium profiles of a droplet on solid surfaces of (a) $\theta^{eq}=30°$, (b) $\theta^{eq}=150°$. Solid lines represent contours of $\rho=0.3,0.6,0.9$ and dashed lines represent the initial location of $(\rho_l^{sat}+\rho_v^{sat})/2=0.6$.

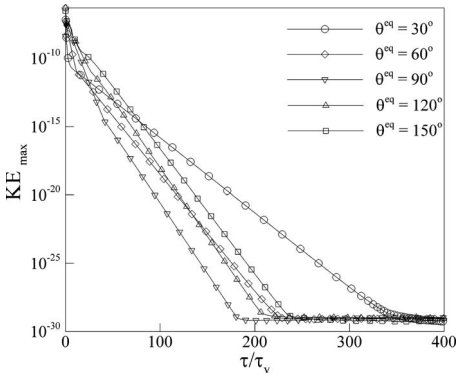

FIG. 2. Time evolution of the maximum kinetic energy with different values of θ^{eq} at $D=4$, $R_{90°}=25$, $\rho_l^{sat}=1.0$, and $\rho_v^{sat}=0.2$. Time is nondimensionalized to the viscous time of the vapor phase $t_v=\rho_v^{sat}\nu_v^{sat}R_{\theta^{eq}}/\sigma$. τ and β are fixed at 0.5 and 0.01, respectively.

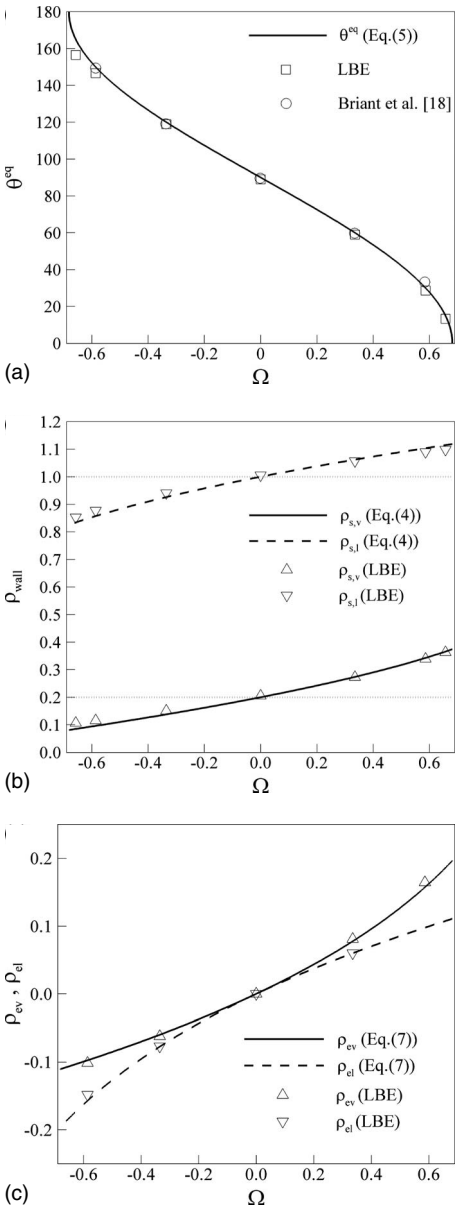

FIG. 3. (a) The equilibrium contact angle θ^{eq}, (b) density at the solid surface, and (c) excess mass vs dimensionless wetting potential Ω. In (b) and (c), solid lines represent the vapor phase and dashed lines represent the liquid phase.

profiles of a droplet sitting on the solid surfaces with the equilibrium contact angles of 30° and 150°. At equilibrium, the parasitic currents drop to round-off. We fix $\beta=0.01$, $\rho_l^{sat}=1.0$, $\rho_v^{sat}=0.2$, and $D=4$, in which case the surface tension force becomes $\sigma=1.365\times10^{-3}$. The dimensionless relaxation time is set to $\tau=\lambda/\delta t=0.5$, where δt is the time step. As an initial condition, a two-dimensional (2D) droplet is generated at the bottom center of the 150×50 computational domain. The initial area of the droplet with different contact angles is kept constant such that its radius on the neutrally wetting solid surface is $R_{90°}=25$. The liquid-vapor interface is represented by a contour level $(\rho_l^{sat}+\rho_v^{sat})/2$ and is found to be well preserved after long time integration.

Two things are notable. First, in Fig. 1(a) the shape of the

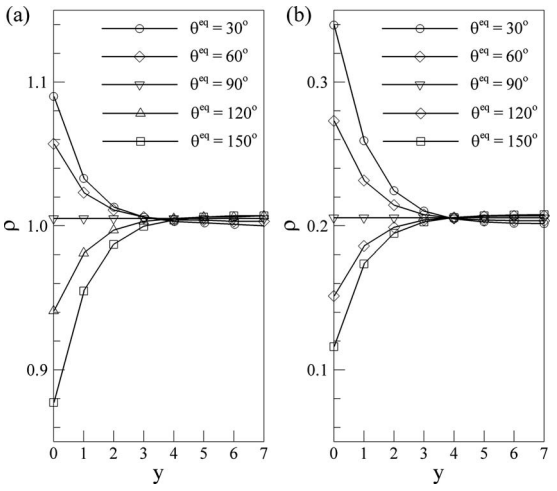

FIG. 4. The density profiles of (a) the liquid and (b) the vapor phases vs the distance y from the wall with different values of θ^{eq}.

contact line near the solid surface is slightly deformed toward the center of the droplet. As will be discussed later, it is because wetting surfaces locally increase the fluid density and therefore the contact line may not be properly represented by the contour level $(\rho_l^{sat}+\rho_v^{sat})/2$. Second, in Fig. 1(b) the droplet radius is apparently reduced from its initial value. It is due to the inclusion of curvature and the consequent elevation of the equilibrium bulk density inside the droplet [5]. The reduction in radius is less pronounced in Fig. 1(a) where the contact angle is smaller and the radius of curvature is larger.

Time evolution of the maximum kinetic energy with different contact angles is shown in Fig. 2. When the time is nondimensionalized to the viscous time of the vapor phase $t_v=\rho_v^{sat}\nu_v^{sat}R_{\theta^{eq}}/\sigma$, the convergence rates for different θ^{eq} roughly collapse on a single curve except for $\theta^{eq}=30°$. At small θ^{eq}, the liquid-vapor interface is too close to the solid surface making it difficult for the liquid at the solid surface to reach the elevated equilibrium density.

Figure 3(a) shows the equilibrium contact angle θ^{eq} vs the dimensionless wetting potential Ω. The equilibrium contact angle is calculated from the geometry of a droplet placed on the solid surface [16]. The LBE simulations are compared with the analytic solution, Eq. (5), and they are in good agreement for moderate contact angles. The LBE results start to deviate from Eq. (6) at large contact angles. It is speculated that since the area of the droplet is fixed in all simulations, the radius of the droplet is smaller for nonwetting surfaces and the grid resolution to represent a droplet is deteriorated as a result. It is noteworthy that neither the density nor the gradient of density at the solid surface is fixed during the simulation. It evolves as part of the solution to minimize the total free energy. If the wall density is prescribed as in the coating approach [27], or $\kappa\mathbf{n}\cdot\nabla\rho_s=-\phi_1$ is enforced for the first derivative of density as well as the second derivative [18], the parasitic currents do not disappear because of redundant boundary conditions, although the equilibrium contact angle still agrees well with theory. In Fig. 3(b), comparison between the surface densities at the solid surface in the LBE simulations and the analytic for-

mula, Eq. (4), is given. On wetting surfaces, fluid densities are elevated as Ω, while on nonwetting surfaces, they are lowered. It can be shown that the density varies exponentially from the value at the solid surface to that in the bulk. The excess mass due to the deviation of the wall density from that of the bulk fluid can be defined as $\rho_{eb}=\int_0^\infty[\rho(y)-\rho_{bulk}]dy$ [17], where $b=v$ (vapor) or l (liquid). For the pseudo–van der Waals fluid, they become

$$\rho_{ev} = -\sqrt{\frac{\kappa}{2\beta}}\ln\frac{1}{2}(1+\sqrt{1-\Omega}),$$

$$\rho_{el} = \sqrt{\frac{\kappa}{2\beta}}\ln\frac{1}{2}(1+\sqrt{1+\Omega}). \tag{7}$$

In Fig. 3(c), the computed values of the excess mass are compared with the analytic prediction. The density of the computed bulk fluid inside the droplet is taken as ρ_{bulk} rather than the saturation density, because of the inclusion of curvature. The density profiles of the liquid along the centerline of the droplet and the vapor along the vertical line away from the droplet are presented in Fig. 4. The exponential variation of the density from the solid surface is clearly visible. Due to the inclusion of curvature, the bulk densities ρ_{bulk} for both liquid and vapor phases are elevated over their saturation densities $\rho_l^{sat}=1.0$ and $\rho_v^{sat}=0.2$. The bulk densities inside and outside of the droplet increase as the radius of curvature of a droplet gets smaller at larger θ^{eq}.

To summarize, we demonstrated that the parasitic currents could be eliminated to round-off if the potential form of the intermolecular force was used with the boundary conditions based on the wall energy approach and the bounce-back rule. The small counter-rotating vortices commonly found near the contact lines are simply numerical artifacts and are eliminated in the proposed approach. The wall energy approach needs to be correctly implemented in the framework of the bounce-back rule. Redundant prescription of boundary conditions does not minimize the total free energy, in which case the LBE method is unable to reach equilibrium.

This work was supported by the startup fund from The City College of the City University of New York.

[1] M. Latva-Kokko and D. H. Rothman, Phys. Rev. Lett. **98**, 254503 (2007).
[2] E. Dussan, J. Fluid Mech. **75**, 609 (1974).
[3] X. Shan, Phys. Rev. E **73**, 047701 (2006).
[4] A. Wagner, Int. J. Mod. Phys. B **17**, 193 (2002).
[5] T. Lee and P. F. Fischer, Phys. Rev. E **74**, 046709 (2006).
[6] S. V. Lishchuk, C. M. Care, and I. Halliday, Phys. Rev. E **67**, 036701 (2003).
[7] P. Lallemand, L.-S. Luo, and Y. Peng, J. Comput. Phys. **226**, 1367 (2007).
[8] M. R. Swift, W. R. Osborn, and J. M. Yeomans, Phys. Rev. Lett. **75**, 830 (1995).
[9] J. Zhang and D. Kwok, Langmuir **20**, 8137 (2004).
[10] S. Mukherjee and J. Abraham, J. Colloid Interface Sci. **312**, 341 (2007).
[11] H. Huang, D. T. Thorne, M. G. Schaap, and M. C. Sukop, Phys. Rev. E **76**, 066701 (2007).
[12] L. Fan, H. Fang, and Z. Lin, Phys. Rev. E **63**, 051603 (2001).
[13] O. Kuksenok, J. M. Yeomans, and A. C. Balazs, Phys. Rev. E **65**, 031502 (2002).
[14] R. Benzi, L. Biferale, M. Sbragaglia, S. Succi, and F. Toschi, Phys. Rev. E **74**, 021509 (2006).
[15] N. S. Martys and H. Chen, Phys. Rev. E **53**, 743 (1996).
[16] Q. Kang, D. Zhang, and S. Chen, Phys. Fluids **14**, 3203 (2002).
[17] P. Papatzacos, Transp. Porous Media **49**, 139 (2002).
[18] A. Briant, P. Papatzacos, and J. Yeomans, Philos. Trans. R. Soc. London, Ser. A **360**, 485 (2002).
[19] A. J. Briant, A. J. Wagner, and J. M. Yeomans, Phys. Rev. E **69**, 031602 (2004).
[20] Y. Yan and Y. Zu, J. Comput. Phys. **227**, 763 (2007).
[21] P. de Gennes, Rev. Mod. Phys. **57**, 827 (1985).
[22] P. Bhatnagar, E. Gross, and M. Krook, Phys. Rev. **94**, 511 (1954).
[23] X. He, X. Shan, and G. Doolen, Phys. Rev. E **57**, R13 (1998).
[24] Y. H. Qian and S. Y. Chen, Phys. Rev. E **61**, 2712 (2000).
[25] D. Jamet, D. Torres, and J. Brackbill, J. Comput. Phys. **182**, 276 (2002).
[26] T. Lee and C.-L. Lin, Phys. Rev. E **71**, 046706 (2005).
[27] M. R. Swift, E. Orlandini, W. R. Osborn, and J. M. Yeomans, Phys. Rev. E **54**, 5041 (1996).